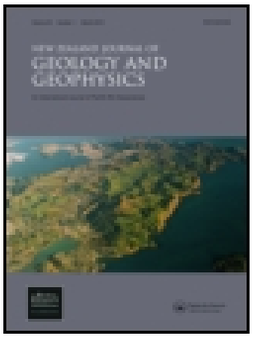

New Zealand Journal of Geology and Geophysics

ISSN: 0028-8306 (Print) 1175-8791 (Online) Journal homepage: http://www.tandfonline.com/loi/tnzg20

Topographic control on shallow fault structure and strain partitioning near Whataroa, New Zealand demonstrates weak Alpine Fault

Phaedra Upton, Bo Ra Song & Peter O. Koons

To cite this article: Phaedra Upton, Bo Ra Song & Peter O. Koons (2017): Topographic control on shallow fault structure and strain partitioning near Whataroa, New Zealand demonstrates weak Alpine Fault, New Zealand Journal of Geology and Geophysics, DOI: 10.1080/00288306.2017.1397706

To link to this article: https://doi.org/10.1080/00288306.2017.1397706

NEW ZEALAND JOURNAL OF GEOLOGY AND GEOPHYSICS, 2017
https://doi.org/10.1080/00288306.2017.1397706

Taylor & Francis
Taylor & Francis Group

RESEARCH ARTICLE

Topographic control on shallow fault structure and strain partitioning near Whataroa, New Zealand demonstrates weak Alpine Fault

Phaedra Upton[a], Bo Ra Song[b] and Peter O. Koons[b,c]

[a]GNS, Lower Hutt, New Zealand; [b]School of Earth and Climate Sciences, University of Maine, Orono, ME, USA; [c]Climate Change Institute, University of Maine, Orono, ME, USA

ABSTRACT
It is notoriously difficult to characterise the strength and stress states of major plate boundaries. By taking advantage of the well-constrained stress contribution of topography adjacent to a segmented section of the Alpine Fault, New Zealand, we have identified a mechanical mix that produces the distinct fault segmentation pattern seen in field observations. Slope-generated shear and normal stresses rotate the principal stresses relative to the regional tectonically derived stress state and under certain strength states influence the displacement pattern. Three-dimensional models show that the scale and form of the near-surface partitioning depend on both topographic relief and local fault strength relative to the bedrock. The models suggest the Alpine Fault is weak to moderately weak relative to the bedrock and is a single structure to within c. 500 m of the surface, above which segmentation occurs. Adjacent to the Alpine Fault, the stress state is highly variable. The intermediate principal stress, σ_2, is rotated from tectonically dominated, near-vertical beneath ridges to near-horizontal beneath large valleys. Individual segments along the Alpine Fault dominated by strike-slip faulting, oblique thrusting or thrusting, can be identified by extracting the topographic contribution to the stress state from numerical models.

ARTICLE HISTORY
Received 29 September 2017
Accepted 25 October 2017

ASSOCIATE EDITOR
Professor Timothy Little

KEYWORDS
Alpine Fault; strain partitioning; topographic stresses; mechanical modelling; stress state

Introduction

The Alpine Fault, which extends along the western edge of the Southern Alps, is the most obvious manifestation of the Australian–Pacific plate boundary through the South Island (Figure 1). It accommodates 65%–75% of the total Australian–Pacific relative plate boundary movement, rupturing episodically in large magnitude earthquakes (M_w c. 8) and appears to be late in its seismic cycle (Sutherland et al. 2007; Howarth et al. 2012, 2016). At scales of tens of kilometres, the Alpine Fault appears to be a remarkably linear feature. Unlike at many oblique plate boundaries (Wentworth and Zoback 1989; McCaffrey 1992, 1996), it accommodates both fault-parallel and fault-normal components of deformation along a single structure through most of the frictional crust (Norris et al. 1990; Koons et al. 2003).

Close to the surface, in the upper kilometre of the crust, the central Alpine Fault becomes segmented (Norris and Cooper 1995, 1997; Barth et al. 2012; Langridge et al. 2014). When first mapping the central section, Norris and Cooper (1995, 1997) proposed 'serial partitioning' to explain their observations that northerly striking sections accommodate oblique thrusting, whereas more easterly striking sections are dominantly dextral strike-slip. This model was in contrast to the more common parallel partitioning where oblique motion is accommodated on parallel thrust and strike-slip faults (Wentworth and Zoback 1989; McCaffrey 1992, 1996). Norris and Cooper (1995) used sandbox models to propose that local stress field perturbations due to the steep range front with deeply incised river valleys promote serial partitioning. The acquisition of airborne light detection and ranging (LiDAR) data has refined these observations and highlighted more parallel partitioning along the fault (Barth et al. 2012; Langridge et al. 2014). Barth et al. (2012) suggest that the style of partitioning and fault segmentation is scale dependent. At the first order (>10^6 to 10^4 m) it is unpartitioned (Koons et al. 2003), at the second order (10^4 to 10^3 m) motion is serially partitioned in the upper c. 1–2 km and at a third order (10^3–10^0 m) it is parallel partitioned into fault wedges in the hanging wall.

Strain partitioning implies local perturbation of the stress state. Field-based studies and LiDAR cannot fully characterise the spatial variation of stress orientations; nor can they define the relative impact of controlling factors including topographic relief and fault strength. The purpose of this article is to use a fully 3D mechanical modelling system to quantify the constraints on strain partitioning and fault segmentation in the near-surface of the Alpine Fault. Our focus is the Whataroa valley where recent drilling to nearly 1 km depth in an attempt to intersect the fault plane revealed unexpected complexity in the valley geometry

CONTACT Phaedra Upton p.upton@gns.cri.nz
Supplemental data for this article can be accessed https://doi.org/10.1080/00288306.2017.1397706.

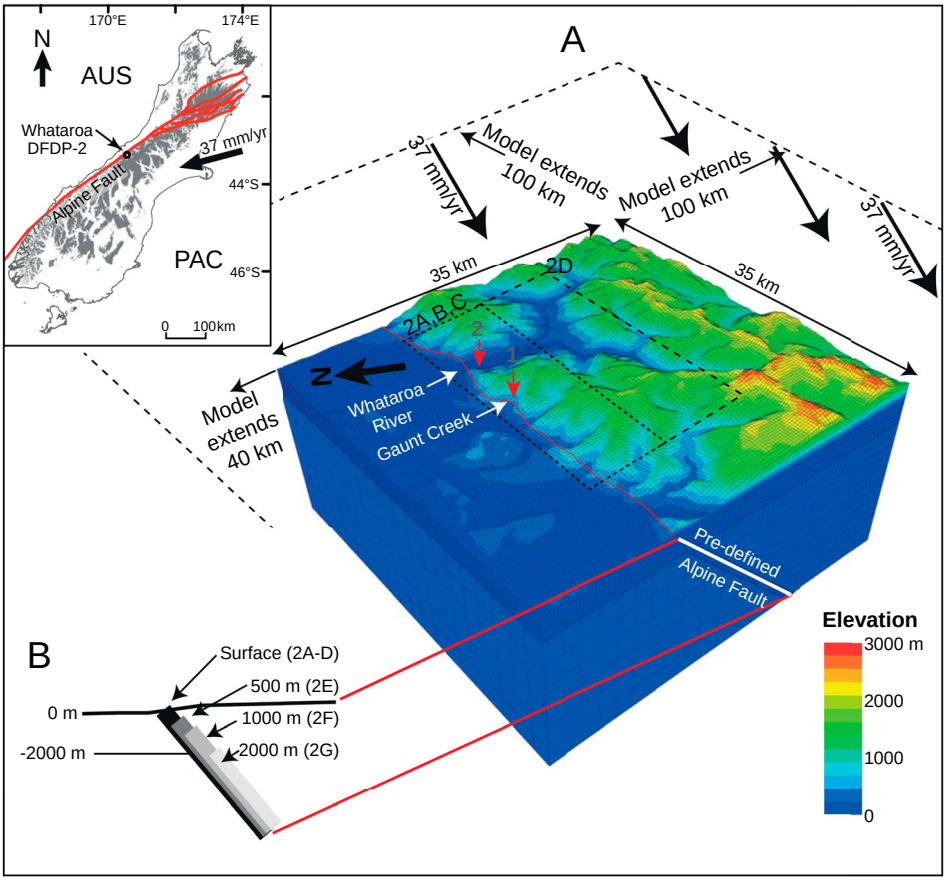

Figure 1. A, Model geometry based on a 200 m digital elevation model (contour interval 200 m) of a 35 × 35 km region including the Whataroa River and Gaunt Creek. The region of interest is embedded into a larger model with dimensions of 175 km × 135 km × 25 km and velocity conditions are imposed on the boundaries as shown by the black arrows. Red arrows show the DFDP-1 and 2 drill holes (Sutherland et al. 2012, 2017). The Alpine Fault is included as a pre-existing weakness dipping at 50° southeast to depths ranging from 0 m to 2000 m. The red line shows the trace of the Alpine Fault from the Active Faults Database (Langridge et al. 2016). Dashed boxes show regions plotted in Figure 2. **B,** Detail of weaker Alpine Fault material, each line is offset for illustrative purposed only, letters in brackets refer to Figure 2. Inset, Plate boundary setting showing the Alpine Fault, Whataroa and the plate motion vector (DeMets et al. 1994).

and potentially the fault as well (Sutherland et al. 2017; Toy et al. 2017). We show that topographic relief, coupled with strain-dependent rheological evolution, perturbs the 3D stress state in the top couple of kilometres, controlling where and how displacement on the Alpine Fault is accommodated in the near-surface and we use this finding to estimate its frictional strength.

Model methodology

To explore the relationships between topographic relief, fault partitioning and fault strength, we solved simultaneously the motion and stress relations for a 3D deforming crust using a field-constrained rheological model. We solved a series of 3D mechanical models using the continuum code FLAC^{3D} (Itasca 2014).

Model geometry and boundary conditions

Our model consists of a high-resolution region (x = 35 km, y = 35 km, depth = 10 km and 200 m resolution) centred on the mouth of the Whataroa gorge, shown in Figure 1(A). This is embedded into a larger low-resolution region which has the dimensions 175 km normal to and 235 km parallel to the Alpine Fault, extending to a depth of 25 km. Only the high-resolution part of the model includes topography (Figure 1A). The model boundaries are placed at a considerable distance from the high-resolution region to ensure that boundary effects do not influence our results. Velocity boundary conditions, derived from GPS and plate reconstructions (DeMets et al. 1994; Wallace et al. 2007) are imposed on the model edges. The material representing the Australian Plate is held still, whereas that representing the Pacific Plate moves at a rate of 37 mm/yr (Figure 1A). All models have a pre-existing dipping (50° southeast) structure representing the Alpine Fault (Figure 1A). The strength of the structure and its initial geometry are varied for different models as described below.

Material properties used in the models

The models assume a two-layered crust, similar to that in previously published modelling studies (Upton and

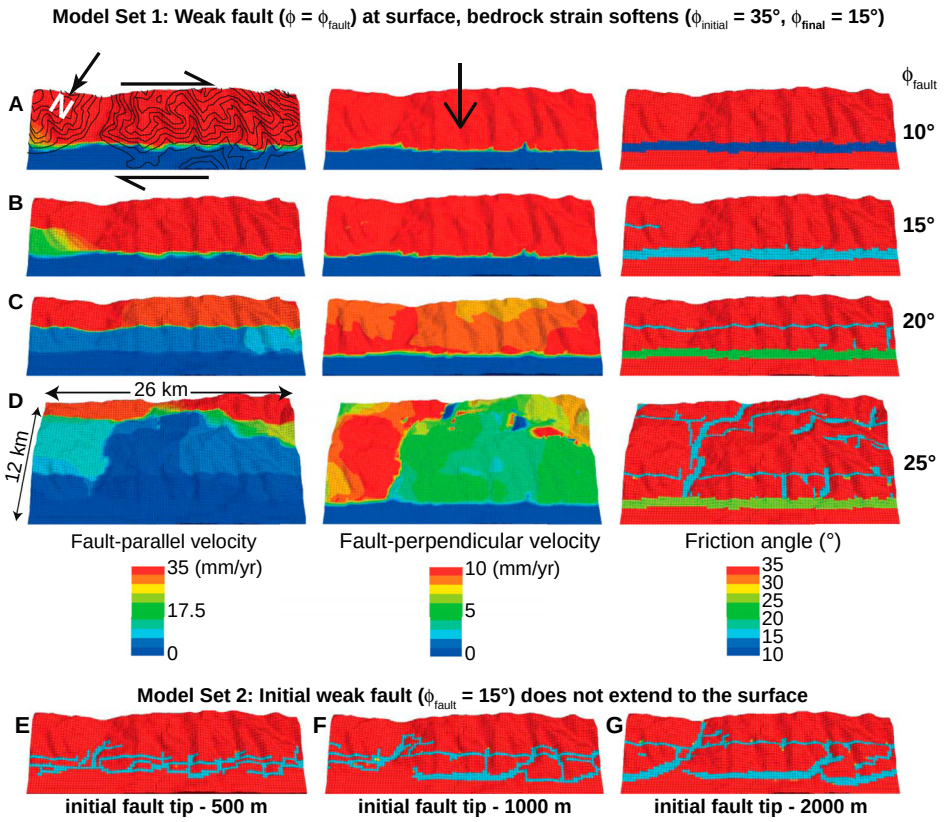

Figure 2. Model results shown as fault-parallel velocity, fault-normal velocity and friction angle (φ) looking down on the models as shown by dashed boxes in Figure 1(A). Note that D includes a larger region as the zones of localisation in this model are more widespread than for A–C. The material strain softens thus φ is representative of strain localisation. **A–D**, The pre-existing Alpine Fault extends to the surface. The black arrows in the left and middle columns of A show the relative motion that each column is illustrating. Boundary parallel or strike-slip motion in the left-hand column and boundary perpendicular or thrust motion in the middle column. A,B, $\varphi = 10$ and 15° respectively. Both fault-parallel and perpendicular velocity components are taken up on that structure. C, $\varphi = 20°$, a vertical structure develops c. 2–3 km southeast of the Alpine Fault which takes up about half of the fault-parallel motion. Fault-normal motion is still taken up along the dipping Alpine Fault. D, $\varphi = 25°$ is unfavourable for fault-parallel motion while half of the fault-normal motion is still taken up along it. Several shear zones develop east of the Alpine Fault. **E–G**, Strain localisation above an initial weak Alpine Fault ($\varphi = 15°$) that extends to within 500 m (F), 1000 m (F) or 2000 m (G) below the surface. In all cases, strain localises onto a series of structures which partition the motion in the near surface.

Koons 2007; Upton et al. 2009; Koons et al. 2012; Roy et al. 2016). We set the model 'frictional viscous transition' 15 km below sea-level (b.s.l.) at a distance from the Alpine Fault and elevated to 10 km b.s.l. adjacent to the fault (Koons 1987; Boese et al. 2012). We use a thermally activated mid-lower crust with material properties identical to previous modelling efforts (Upton and Koons 2007; Upton et al. 2009; Koons et al. 2012; and references therein). The upper crust of the hanging wall is modelled using a strain-softening elastoplastic Mohr–Coulomb rheology based on measured fault rock strength from Haast Schist at the Cromwell Gorge in central Otago (Thomson 1993). This material has an initial friction angle (φ) of 35°, cohesion of 50 MPa, and the capacity to strain soften to a friction angle of 15° and cohesion of 100 kPa after 3% total strain (Thomson 1993; Koons et al. 2012; Roy et al. 2016). The friction angle of the pre-existing model Alpine Fault is varied in the models from 10° to 25°. The friction angle is a measure of the shear strength of a material, measuring its resistance to sliding. In this study, we are interested in the relative strengths of the deformed (faulted) rock and undeformed hanging wall, and their evolution. The strain softening nature of the material modelled means there is a direct relationship between the amount of deformation (faulting) and the final value of the friction angle. For this reason, we use the friction angle (as a measure of strength) to illustrate where faulting has occurred in the models (Figure 2, 3).

Interpreting models of a highly evolved system, such as valley/ridge topography and segmentation along the Alpine Fault, is challenging because we need to strike a balance between over- and under-defining the constraints on the models. In this case, we know that the Alpine Fault is segmented in the uppermost crust and we have hypothesised that both fault strength and topography play a role in determining the nature of the segmentation. If we predefine the fault structure completely, we cannot watch its evolution. However, we need to pre-define enough of the fault structure for the deformation to occur in the areas that we

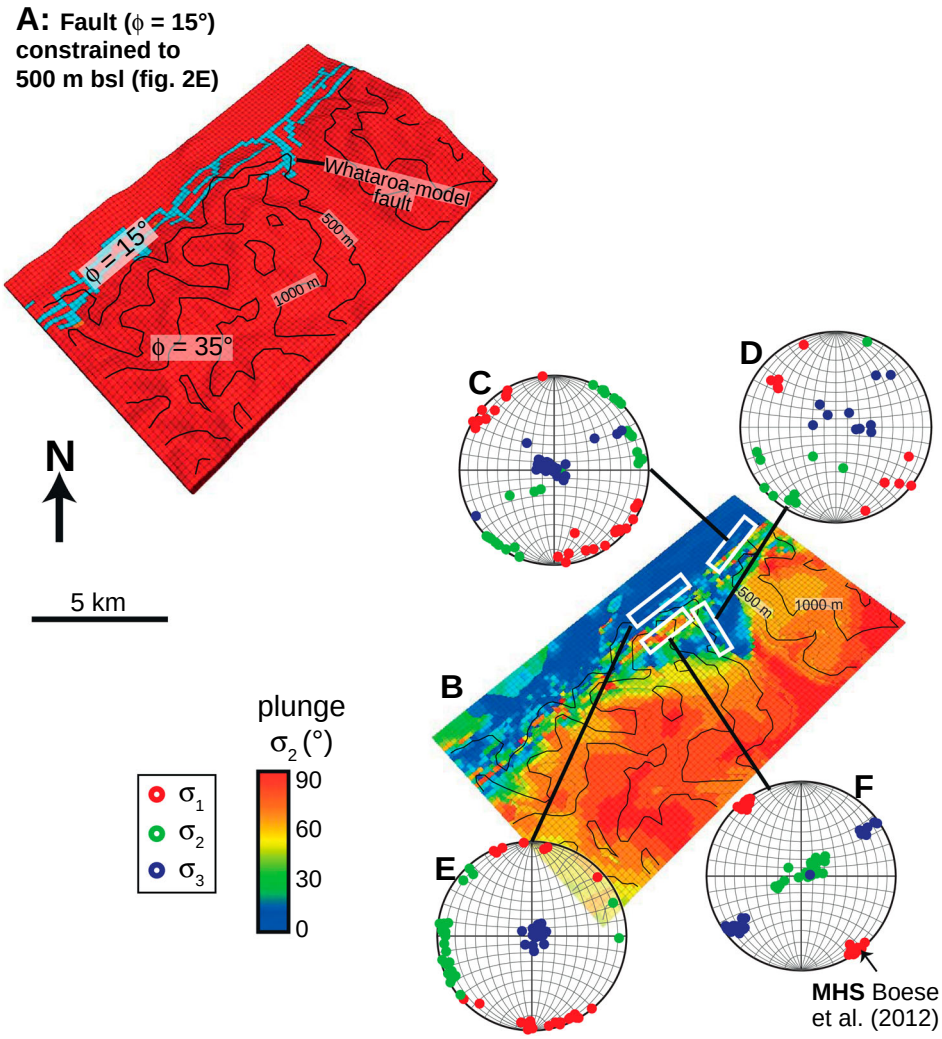

Figure 3. A, The friction angle at the surface above an initial planar Alpine Fault weakness extending to 500 m b.s.l. Light blue: where the hanging wall has strain softened to $\varphi = 15°$, shows the location of high strain zones in the models. **B,** Plunge of σ_2 on a horizontal slice at sea-level though the model shown in A. Blue: σ_2 is near horizontal. Red: σ_2 is near vertical. **C–F,** Stereonet plots showing the stress state within regions outlined by the white boxes. C,E, Thrust segments close to the range front. D, Whataroa-model fault which forms as an oblique sinistral strike-slip structure along the western edge of the Whataroa Valley. F, A strike-slip segment where motion is partitioned between here and the thrust segment shown in E. MHS = Maximum horizontal stress determined by Boese et al. (2012).

know it does. We ran two sets of models to try and unpack these different controls.

Model Set 1 was aimed at the impact of fault strength on the development of strain localisation and fault segmentation. In these models, the pre-existing structure representing the Alpine Fault extends all the way to the surface. Its friction angle was varied from 10° to 25°. These geometries were run to explore how weak a dipping structure must be for both components of deformation—fault normal and fault parallel—to be taken up along it. Models that produced strain patterns unlike those observed along the Alpine Fault tell us what rheological parameters are unlikely.

We then reduced the number of constraints on the models in Model Set 2. These models were run to explore the evolution of strain partitioning and fault segmentation relative to topography and fault strength. To do so, we varied the friction angle as above. We also varied the depth to which the weakness extends toward the surface from 2000 m b.s.l. to 500 m b.s.l. (Figure 1B) to explore the development of fault segmentation relative to topography. These models are not meant to imply that the Alpine Fault suddenly goes from weak to strong in the shallow crust. They are designed so that we can observe how near-surface fault segmentation develops in the absence of pre-defined weaknesses at the surface. We varied the depth of the tip of the pre-defined Alpine Fault to find the model that most closely matches field observations. By using a strain softening rheology for the hanging wall material, we can see where strain is localised in relation to other features in the model.

Model limitations

The resolution of the central part of the models is 200 m, thus we can explore localisation of deformation

only at scales > 200 m. We are unable to model features such as the anisotropy of the schist, the width of the fault damage zone or the footwall rheology. The latter two were called upon by Barth et al. (2012) as constraints on partitioning and the geometry of the hanging wall fault wedges. Our resolution is too coarse to resolve sediments thicknesses of <50–200 m. We also make assumptions about initial conditions and geometries. To avoid complex and difficult to code geometries, which can lead to numerical instabilities, we assume that the Alpine Fault can be modelled as a straight line at 2 km or 500 m b.s.l. in Model Set 2. Given the non-linear nature of the range front at this scale, this is obviously a simplification and we note that in comparing our results with field observations. Finally, no surface processes are imposed in the models.

Model results

Model Set 1

Varying the friction angle of the pre-defined weakness representing the Alpine Fault had a significant impact on the nature of strain partitioning. A weak structure ($\varphi = 10$ or 15°) precludes any partitioning (Figure 2A, B) with both fault-parallel and fault-normal velocity components taken up along this weak structure, whereas a stronger ($\varphi = 25°$) dipping structure took up almost none of the fault-parallel velocity and only a portion of the fault-normal velocity (Figure 2D). In the strong fault case, a series of structures developed in the hanging wall, some parallel to the model Alpine Fault and others at a high angle to it, generally along topographic lows. Fault-parallel motion was largely taken up on two structures, one 2–3 km inboard of the Alpine Fault and a series of sub-parallel high strain zones 8–10 km inboard which form in the upper Whataroa and its tributaries. A second structure developed along the western side of the Whataroa valley (referred to as the Whataroa-model fault). It took up both strike-slip (sinistral) and reverse motion perpendicular to the model Alpine Fault.

Model Set 2

In this model set, we explored the development of partitioning relative to topography by varying the depth to which we pre-define the Alpine Fault weakness. As discussed above, this is not because we think that the Alpine Fault suddenly strengthens in the near-surface, but so that we can observe how fault segmentation evolves unconstrained by pre-existing weaknesses. Boundary-parallel motion was taken up on vertical structures that develop in the hanging wall above the top of the pre-defined weakness. Where this depth is greater, vertical structures developed further from the range front (Figure 2E–G; Figures S1–S3). The boundary-normal component was influenced by the topographic relief, especially where the depth to the top of the pre-defined model Alpine Fault is greater (Figures S1–S3). Structures developed along the edge of the Whataroa and Waitangitaona valleys, which take up a considerable portion of the boundary-normal deformation. These structures are seen in the φ plots as zones of weakness that curve into the river valleys from the north (Figures S1–S3).

Discussion

Partitioning of strain and segment characteristics

Varying the strength of the Alpine Fault and the depth of the pre-defined weak dipping structure in the models produced a variety of patterns of strain localisation at the surface. As the strength ratio between the bedrock and the model Alpine Fault decreased or the up-dip top of the pre-defined weak dipping structure was at greater depth, the development of vertical, dominantly strike-slip structures developed further southeast of the Alpine Fault. Under these conditions, the Alpine Fault is not favourably oriented to take up the highly oblique motion and deformation is strongly partitioned. Field observations and LiDAR suggest, based on the assumption that thrust segments dip at c. 45° and strike-slip segments are close to vertical, that strain partitioning in the shallow brittle crust is restricted to within c. 500 m of the range front (Barth et al. 2012; Langridge et al. 2014). Vertical strike-slip sections found crossing the toe of ridges c. 500 m inboard of the range front strongly suggest that individual structures merge into a single structure at shallow depths (Norris and Cooper 1995, 1997; Barth et al. 2012; Langridge et al. 2014). The field observations best fit a model with a single weak fault plane to c. 500 m b.s.l. and segmentation of the fault into shallow vertical and dipping structures at about this depth. A comparison with structures mapped from LiDAR also suggests this depth is <500 m (Figure 4). Our model cannot capture all the complexity of the natural system and assumes that the Alpine Fault at depth is planar. Where our model deviates most from the mapped features, northeast of Gaunt Creek, it is possible that the weak Alpine Fault in the near-surface extends further northwest than in our simplified model geometry (Figure 4).

Stress state in the near-surface and its relationship to topography

The model stress state varies along strike (Figure 3; Figure S4). Beneath the ridges, the stress state is close to the regional stress regime where σ_2 is near

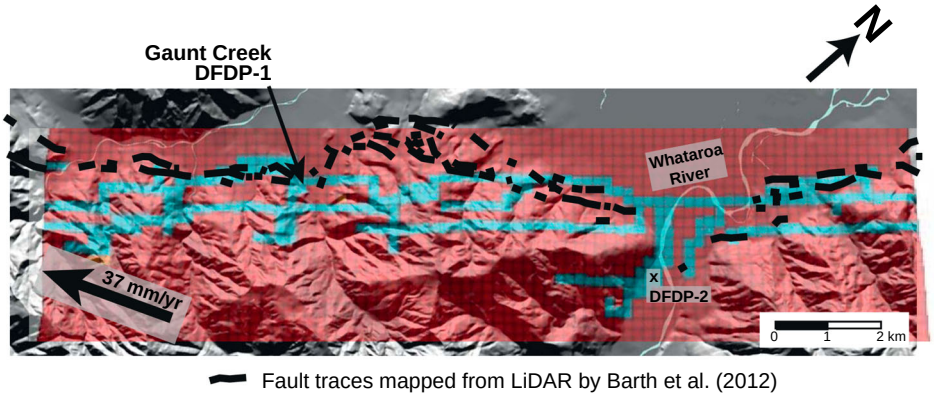

Figure 4. Comparison of model (Figure 3A) results with LiDAR observations (from Barth et al. 2012).

vertical, i.e. far-field tectonic driving forces dominate the stress regime (Koons 1994; Boese et al. 2012). Beneath the valleys, the intermediate principal stress, σ_2, is rotated to near-horizontal by the topographic relief, reflecting a thrust stress regime rather than oblique strike-slip. Along the model Alpine Fault, we observe rotation of the stress state and partitioning of deformation onto oblique thrust and oblique strike-slip structures. At the valley mouth, a thrust segment curves into the valley and the stress state is one of almost pure thrusting (Figure 3C). Along strike to the south, parallel partitioning is obvious with a strike-slip segment (Figure 3F) and a thrust segment (Figure 3E). σ_1 for this segment is very close to the regional maximum horizontal stress observed by Boese et al. (2012). As well as rotation of the stress state, field observations from Franz Josef, 20 km south of our field area, suggest that the magnitudes of the σ_2 and σ_3 are close and readily switch (Enlow and Koons 1998). The youngest shallow-level vein sets in the Franz Josef river valley are both sub-horizontal and sub-vertical and these two sets are mutually cross-cutting. This implies that σ_2 and σ_3 are of similar magnitude and there was some switching between the two in the deformation history (Hanson et al. 1990).

The Whataroa valley and its tributaries are the largest erosional hole along the western Southern Alps, representing a major departure from the dominant topography of the steep and high Southern Alps. We might expect to see rotation of the stress state and strain concentration along the Whataroa, as a consequence of slope-generated shear and normal stresses which reduce the amount of tectonic stress required to reach failure (Koons and Kirby 2007). Where the Alpine Fault is strong ($\varphi = 20$ or 25°), our models do predict significant perturbation of the stress state. They also predict that tectonic stresses in the hanging wall combine with slope-generated stresses to form a structure we have called the Whataroa-model fault, which extends c. 10 km along the western Whataroa valley (Figure S3).

Controls on the strength of the shallow Alpine Fault

The lack of field evidence for (1) major active structures parallel to the large valleys, and (2) vertical strike-slip structures at distances > 500 m from the range front provides a robust constraint on the strength of the Alpine Fault. The lack of these two suggest the Alpine Fault is sufficiently weak ($\varphi < 20°$) that the topographic stress perturbation of the Whataroa valley and its tributaries is insufficient to shift significant failure away from the dipping fault plane. In these models, tectonic stresses in the hanging wall still combine with slope-generated stresses to form a shorter version of the Whataroa-model fault (Figure 3) which extends c. 2 km along the western Whataroa valley. This modelled structure is predicted to have minor oblique sinistral strike-slip motion, up to the east (Figure 3D; Figure S1). A structure such as this might explain the bedrock geometry at the DFDP-2B drill site where the depth to basement far exceeded expectations (Sutherland et al. 2017). This could be due to one or both of the following processes. Motion along the structure dropping the western side of the valley down relative to the eastern side or enhanced erosion of a weakened fault zone by successive glaciations during the Pleistocene resulting in an over-steepened valley (Roy et al. 2015).

Comparison with other models

Barth et al. (2012) propose that the width, extent and geometry of the fault wedges are controlled by the thickness of the footwall sediments and the width of the fault damage zone. We cannot test these two attributes as constraints because the resolution of our models is too coarse to include them. We do show that stress perturbations, which result from topography, as first mooted by Norris and Cooper (1995, 1997), produce a combination of serial and parallel partitioning along the range front of the Southern Alps. We would argue that it is not necessary to appeal to footwall rheology to explain the observations, but we cannot discount the suggestion that it does play a role

in controlling the details of individual fault segments, as suggested previously (Barth et al. 2012). Our models differ from Norris and Cooper (1995, 1997) in that they have no pure strike-slip segments, instead a combination of serial and parallel partitioning develops, as also noted by Langridge et al. (2014) in their interpretation of LiDAR observations.

Conclusions

In mountainous regions, topography perturbs the stress state, and couples with rheology to influence the localisation of strain, particularly in regions of oblique deformation. We used 3D mechanical models to show that as the strength ratio between the bedrock and an oblique dipping fault is decreased, or the depth to the up-dip tip of a single weak dipping structure is increased, two effects are observed. First, vertical, dominantly strike-slip structures develop further and further into the hanging wall. Second, strain is localised into significant topographic perturbations. We use field and LiDAR observations, our 3D models and the perturbation to the stress field from topography to evaluate the strength and stress regime of the Alpine Fault. A strong model Alpine Fault or a situation where boundary-parallel motion is able to bleed off a single dipping structure onto vertical strike-slip faults at depths >500 m does not match the observations. A weak model Alpine Fault, which is a single structure at depths >500 m, predicts that both vertical strike-slip structures and structures following topographic lows are restricted to within c. 500 m of the range front, consistent with field and LiDAR observations. At shallower depths, rather than pure serial or parallel partitioning occurring, the interaction of a weak fault and the topography produces a complex pattern that is a combination of both serial and parallel partitioning. Strike-slip segments occur within the hanging wall of the range front, while oblique thrusting is taken up at the range front.

Acknowledgements

The models and analysis presented in this manuscript are built on the considerable contribution of the late Richard Norris to our understanding the Alpine Fault and we are grateful for the many discussions with Richard over several years. We also acknowledge useful feedback and discussions with Alan Cooper, Rupert Sutherland and Susan Ellis. Tim Little, Rob Langridge, Virginia Toy and two anonymous reviewers all provided constructive feedback. Nick Mortimer is thanked for his editorial oversight.

Disclosure statement

No potential conflict of interest was reported by the authors.

Funding

This work was supported by the NZ Ministry for Business Innovation and Employment and National Science Foundation grants 1009626 and 1324637 to P. O. Koons; Division of Earth Sciences.

References

Barth NC, Toy VG, Langridge RM, Norris RJ. 2012. Scale dependence of oblique plate-boundary partitioning: New insights from LiDAR, central Alpine Fault, New Zealand. Lithosphere. 4:435–448.

Boese CM, Townend J, Smith EGC, Stern T. 2012. Microseismicity and stress in the vicinity of the Alpine Fault, central Southern Alps, New Zealand. Journal of Geophysical Research. 117:B02302.

DeMets C, Gordon RG, Argus DF, Stein S. 1994. Effect of recent revisions to the geomagnetic reversal time scale on estimates of current plate motions. Geophyiscal Research Letters. 21:2191–2194.

Enlow RL, Koons PO. 1998. Critical wedges in three dimensions: analytical expressions from Mohr-Coulomb constrained perturbation analysis. Journal of Geophysical Research-Solid Earth. 103:4897–4914.

FLAC3D (Fast Lagrangian Analysis of Continua in 3 Dimensions) User's Guide [2014. Version 5.1. Minneapolis, Minnesota: Itasca Consulting Group Inc.

Hanson CR, Norris RJ, Cooper AF. 1990. Regional fracture patterns east of the Alpine Fault between the Fox and Franz Josef Glaciers, Westland, New Zealand. New Zealand Journal of Geology & Geophysics. 33:617–622.

Howarth JD, Fitzsimons SJ, Norris RJ, Jacobsen GE. 2012. Lake sediments record cycles of sediment flux driven by large earthquakes on the Alpine Fault, New Zealand. Geology. 40:1091–1094.

Howarth JD, Fitzsimons SJ, Norris RJ, Langridge R, Vandergoes MJ. 2016. A 2000 yr rupture history for the Alpine Fault derived from Lake Ellery, South Island, New Zealand. Bulletin of the Geological Society of America. 128:627–643.

Koons PO. 1987. Some thermal and mechanical consequences of rapid uplift: an example from the Southern Alps, New Zealand. Earth and Planetary Science Letters. 86:307–319.

Koons PO. 1994. Three-dimensional critical wedges: tectonics and topography in oblique collisional orogens. Journal of Geophysical Research. 99:12301–12315.

Koons PO, Kirby E. 2007. Topography, denudation, and deformation. The role of surface processes in fault evolution. In: Tectonic faults; agents of change on a dynamic earth. Cambridge: MIT Press; p. 205–230.

Koons PO, Norris RJ, Craw D, Cooper AF. 2003. Influence of exhumation on the structural evolution of transpressional plate boundaries: an example from the Southern Alps, New Zealand. Geology. 31:3–6.

Koons PO, Upton P, Barker AD. 2012. The influence of mechanical properties on the link between tectonic and topographic evolution. Geomorphology. 137:168–180.

Langridge RM, Ries WF, Farrier T, Barth NC, Khajavi N, De Pascale GP. 2014. Developing sub 5-m LiDAR DEMs for forested sections of the Alpine and Hope faults, South Island, New Zealand: implications for structural interpretations. Journal of Structural Geology. 64:53–66.

Langridge RM, Ries WF, Litchfield NJ, Villamor P, Van Dissen RJ, Barrell DJA, Rattenbury MS, Heron DW, Haubrock S, Townsend DB, et al. 2016. The New

Zealand Active Faults Database. New Zealand Journal of Geology and Geophysics. 59:86–96.
McCaffrey R. 1992. Oblique plate convergence, slip vectors, and forearc deformation. Journal of Geophysical Research. 97:8905–8915.
McCaffrey R. 1996. Slip partitioning at convergent plate boundaries of SE Asia. In: Geological Society Special Publication. p. 3–18.
Norris RJ, Cooper AF. 1995. Origin of small-scale segmentation and transpressional thrusting along the Alpine Fault, New Zealand. Geological Society of America Bulletin. 107:231–240.
Norris RJ, Cooper AF. 1997. Erosional control on the structural evolution of a transpressional thrust complex on the Alpine Fault, New Zealand. Journal of Structural Geology. 19:1323–1342.
Norris RJ, Koons PO, Cooper AF. 1990. The obliquely-convergent plate boundary in the South Island of New Zealand: implications for ancient collision zones. Journal of Structural Geology. 12:715–725.
Roy SG, Koons PO, Upton P, Tucker GE. 2015. The influence of crustal strength fields on the patterns and rates of fluvial incision. Journal of Geophysical Research: Earth Surface. 120:275–299.
Roy SG, Koons PO, Upton P, Tucker GE. 2016. Dynamic links among rock damage, erosion, and strain during orogenesis. Geology. 44:583–586.
Sutherland R, Eberhart-Phillips D, Harris RA, Stern T, Beavan J, Ellis S, Henrys S, Cox S, Norris RJ, Berryman KR, et al. 2007. Do great earthquakes occur on the Alpine Fault in the Central South Island, New Zealand? In: A continental plate boundary: tectonics at South Island, New Zealand. Washington (DC): AGU; p. 235–251.
Sutherland R, Townend J, Toy V, Upton P, Coussens J, Allen M, Baratin L-M, Barth N, Becroft L, Boese C, et al. 2017. Extreme hydrothermal conditions at an active plate-bounding fault. Nature. 06/01/print;546:137–140.
Thomson R. 1993. Clyde Dam Engineering Geological Completion Report Volume 1: Text and Appendices. Institute of Geological and Nuclear Sciences science report 94/33.
Toy VG, Sutherland R, Townend J, Allen MJ, Becroft L, Boles A, Boulton C, Carpenter B, Cooper A, Cox SC, et al. 2017. Bedrock geology of DFDP-2B, central Alpine Fault, New Zealand. New Zealand Journal of Geology and Geophysics. 60:497–518.
Upton P, Koons PO. 2007. Three-dimensional geodynamic framework for the Central Southern Alps, New Zealand: integrating geology, geophysics and mechanical observations. In: A continental plate boundary: tectonics at South Island, New Zealand. Washington (DC): American Geophysical Union; p. 253–270.
Upton P, Koons PO, Craw D, Henderson CM, Enlow R. 2009. Along-strike differences in the Southern Alps of New Zealand: consequences of inherited variation in rheology. Tectonics. 28:TC2007.
Wallace LM, Beavan J, McCaffrey R, Berryman K, Denys P. 2007. Balancing the plate motion budget in the south island, New Zealand using GPS, geological and seismological data. Geophysical Journal International. 168:332–352.
Wentworth CM, Zoback MD. 1989. The style of late Cenozoic deformation at the eastern front of the California coast ranges. Tectonics. 8:237–246.